

Radial buoyancy effects on momentum and heat transfer in a circular Couette flow

Changwoo Kang, Antoine Meyer, and Innocent Mutabazi*

Laboratoire Ondes et Milieux Complexes (LOMC), UMR 6294, CNRS-Université du Havre, Normandie Université, 53 Rue de Prony, CS 80540, 76058 Le Havre CEDEX, France

Harunori N. Yoshikawa

Laboratoire J.-A. Dieudonné, UMR 7351, CNRS-Université Côte d'Azur, Parc Valrose, 06108 Nice Cedex 02, France

(Received 8 October 2016; published 5 May 2017)

The numerical investigation of a circular Couette flow with a radial temperature gradient is performed to elucidate the influence of the radial buoyancy on flow and heat transfer for different values of the Prandtl number when the gravitational acceleration is neglected. We consider an infinite-length cylindrical annulus of radius ratio 0.8 with the inner rotating cylinder and the outer stationary cylinder. The flow is stabilized with the outward heating while it is destabilized with the inward heating. A weakly nonlinear analysis shows that the transition to stationary axisymmetric modes is supercritical while the oscillatory axisymmetric modes occur via a subcritical bifurcation. The effect of the centrifugal buoyancy on the transfer of angular momentum (i.e., torque) is quite weak while the effect on the heat transfer is significant.

DOI: [10.1103/PhysRevFluids.2.053901](https://doi.org/10.1103/PhysRevFluids.2.053901)

I. INTRODUCTION

The flow inside a cylindrical annulus with rotating inner cylinder and stationary outer cylinder subject to a radial temperature gradient has been actively investigated since a few decades ago [1–14], because of its many industrial applications such as cooling of rotating machinery, solidification of pure metals, centrifugation, and chemical vapor deposition. This flow can also be used as a model of the complex geophysical and astrophysical flows in the neighborhood of the equator of planets and stars [15,16].

The geometry of a cylindrical annulus (Fig. 1) is described by the following parameters: the radius ratio $\eta = r_i/r_o$ and the aspect ratio $\Gamma = L/d$, where r_i and r_o are the radii of the inner and outer cylinders, L is the annulus length, and $d = r_o - r_i$ is the annulus width. The fluid has the density ρ , the kinematic viscosity ν , and the thermal diffusivity κ . In the Boussinesq approximation, the density of the fluid is approximated by a linear function of the temperature $\rho(T) \approx \rho_0[1 - \alpha(T - T_0)]$ in driving force terms of the flow equations while it is assumed constant, as the diffusion properties ν and κ , in other terms. Here ρ_0 is the density at a reference temperature T_0 and α is the thermal expansion coefficient. The Prandtl number $\text{Pr} = \nu/\kappa$ and the thermal expansion parameter $\gamma_a = \alpha\Delta T$ are constructed from these properties to characterize the fluid under an imposed temperature difference ΔT .

The stability of the flow with a radial temperature gradient in a cylindrical annulus in negligible gravity field has been studied analytically, in order to recognize the effect of temperature gradient on the flow instability. Becker and Kaye [1] found that the flow is stabilized by heating the inner cylinder, while it is destabilized by heating the outer cylinder. Takhar *et al.* [3] observed that the critical Taylor number (Ta_c) decreases rapidly with increasing the Rayleigh number in the flow

*innocent.mutabazi@univ-lehavre.fr

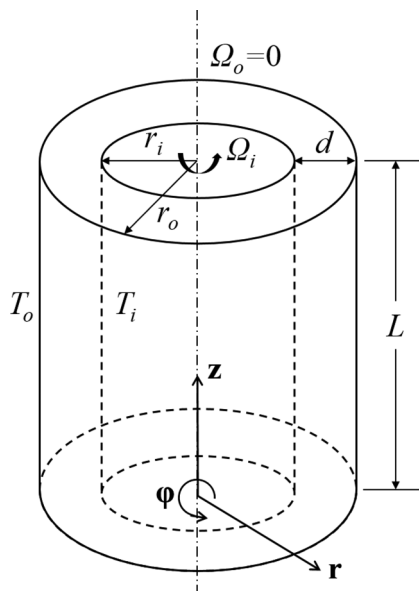


FIG. 1. Sketch of the flow configuration.

between counter-rotating cylinders. Since then, Takhar *et al.* [6] confirmed that the flow is more stable in both corotating and counter-rotating cylinders configurations, when the temperature of the inner cylinder is higher than that of the outer cylinder. Critical wave number also increases steeply by heating the inner cylinder in a counter-rotating configuration. Ali and Weidman [7], Soundalgekar *et al.* [8], Kong and Liu [9], and Jenny and Nsom [10] showed that the critical values of Taylor number and wave number depend on the flow geometry and the thermal variation of fluid properties. Recently, Meyer *et al.* [14] performed a linear stability analysis (LSA) to extend previous studies and to investigate the effect of the radial buoyancy, i.e., a thermal buoyancy force associated with the centrifugal acceleration field [11–14], revealing that critical modes depend on the dimensionless parameters: η , Pr , and γ_a through a single dimensionless number $S = -\gamma_a \text{Pr} / \ln \eta$.

All the above cited studies have revealed the role of the centrifugal buoyancy on the flow stability: it induces the dissymmetry in the threshold and in the nature of the critical modes: the inward heating (i.e., with the cooled inner cylinder) is destabilizing and leads to stationary axisymmetric modes while the outward heating (i.e., with the cooled outer cylinder) is stabilizing and can yield oscillatory modes depending on the values of the number S as proved by a recent analytical study of Kirillov and Mutabazi [17] in a short wavelength approximation.

In the present study, we carry out a numerical investigation on circular Couette flow with a radial temperature gradient to clarify the effect of the radial buoyancy on the flow structure and heat transfer. This is an extension of the work of Meyer *et al.* [14]: the eigenvalue spectrum of the linearized operator is analyzed, and the linear coefficients of the Ginzburg-Landau equation (GLE) are computed for different control parameters (Pr , γ_a) for a fixed value of η ($=0.8$). These results are completed by a DNS (direct numerical simulation) performed with adopting periodic boundary conditions in the axial direction. The DNS code is validated by the comparison of the computed critical values of flow parameters with the predictions of the LSA [14]. Velocity, vorticity, and temperature fields are computed together with the momentum and heat transfer coefficients.

The paper is organized as follows: in Sec. II, the flow geometry and the governing equations are presented together with the adopted numerical methods for their solving. The results are described in Sec. III and discussed in Sec. IV. The last section contains conclusions.

II. PROBLEM FORMULATION

We consider the incompressible flow of a Newtonian fluid in a cylindrical annulus of radius ratio $\eta = 0.8$ (Fig. 1) with rotating inner cylinder at an angular frequency Ω_i and with stationary outer cylinder ($\Omega_o = 0$). The two cylinders are maintained at different constant temperatures T_i and T_o , creating a radial temperature gradient acting on the fluid layer. The temperature difference $\Delta T = T_i - T_o$ is assumed to be small enough for the validity of the Boussinesq approximation.

A. Governing equations

The conservation of mass, momentum, and energy is expressed through the continuity, Navier-Stokes, and energy equations, which relate the velocity \mathbf{u} , the pressure $p = \rho_0\pi$, and the temperature deviation θ from the reference temperature T_o , i.e., $\theta = T - T_o$. In cylindrical coordinates (r, φ, z) these equations read [12–14]

$$\frac{1}{r} \frac{\partial(ru_r)}{\partial r} + \frac{1}{r} \frac{\partial u_\varphi}{\partial \varphi} + \frac{\partial u_z}{\partial z} = 0, \quad (1a)$$

$$\frac{\partial u_r}{\partial t} + (\mathbf{u} \cdot \nabla)u_r - \frac{u_\varphi^2}{r} = -\frac{\partial \pi}{\partial r} + \nu \left(\Delta u_r - \frac{u_r}{r^2} - \frac{2}{r^2} \frac{\partial u_\varphi}{\partial \varphi} \right) - \alpha \theta \mathbf{g}_c, \quad (1b)$$

$$\frac{\partial u_\varphi}{\partial t} + (\mathbf{u} \cdot \nabla)u_\varphi + \frac{u_r u_\varphi}{r} = -\frac{1}{r} \frac{\partial \pi}{\partial \varphi} + \nu \left(\Delta u_\varphi - \frac{u_\varphi}{r^2} + \frac{2}{r^2} \frac{\partial u_r}{\partial \varphi} \right), \quad (1c)$$

$$\frac{\partial u_z}{\partial t} + (\mathbf{u} \cdot \nabla)u_z = -\frac{\partial \pi}{\partial z} + \nu \Delta u_z, \quad (1d)$$

$$\frac{\partial \theta}{\partial t} + (\mathbf{u} \cdot \nabla)\theta = \kappa \Delta \theta, \quad (1e)$$

where (u_r, u_φ, u_z) are the radial, azimuthal, and axial components of \mathbf{u} and differential operators $\mathbf{u} \cdot \nabla$ and Δ are $\mathbf{u} \cdot \nabla = u_r \frac{\partial}{\partial r} + \frac{u_\varphi}{r} \frac{\partial}{\partial \varphi} + u_z \frac{\partial}{\partial z}$ and $\Delta = \frac{1}{r} \frac{\partial}{\partial r} \left(r \frac{\partial}{\partial r} \right) + \frac{1}{r^2} \frac{\partial^2}{\partial \varphi^2} + \frac{\partial^2}{\partial z^2}$. The last term in the right-hand side of Eq. (1b) represents the centrifugal buoyancy per mass unit, which results from the coupling between the temperature gradient and the centrifugal acceleration $\mathbf{g}_c = (u_r^2/r)\mathbf{e}_r$. The kinematic and thermal boundary conditions at the cylindrical surfaces are

$$\mathbf{u} = r_i \Omega_i \mathbf{e}_\varphi, \quad \theta = \Delta T \quad \text{at } r = r_i; \quad \mathbf{u} = 0, \quad \theta = 0 \quad \text{at } r = r_o. \quad (2)$$

In the following, lengths are scaled by the gap width (d), flow velocities by the rotation velocity of the inner cylinder ($r_i \Omega_i$), and the temperature field by the temperature difference (ΔT). The resulting control parameters are the Prandtl number Pr , the radius ratio η , the thermal expansion parameter γ_a , and the Taylor number defined as $\text{Ta} = \text{Re} \sqrt{d/r_i}$, where $\text{Re} = r_i \Omega_i d / \nu$ is the Reynolds number.

The system of Eqs. (1) possesses a base state solution which is stationary and invariant in both axial and azimuthal directions [14]:

$$V(r) = Ar + \frac{B}{r}, \quad \Theta(r) = \frac{\ln(1-\eta)r}{\ln \eta}, \quad A = -\frac{\eta}{1+\eta}, \quad B = \frac{\eta}{(1-\eta)(1-\eta^2)}. \quad (3)$$

The full solution can be cast in the form

$$\begin{pmatrix} \mathbf{u}(t, \mathbf{r}) \\ p(t, \mathbf{r}) \\ \theta(t, \mathbf{r}) \end{pmatrix} = \begin{pmatrix} V(r)\mathbf{e}_r \\ P(r) \\ \Theta(r) \end{pmatrix} + \begin{pmatrix} \mathbf{u}'(t, \mathbf{r}) \\ p'(t, \mathbf{r}) \\ \theta'(t, \mathbf{r}) \end{pmatrix}, \quad (4)$$

where $(\mathbf{u}', p', \theta')$ are perturbation velocity, pressure, and temperature fields around the base flow (3).

The substitution of Eq. (4) into Eqs. (1) yields

$$\mathbf{L}(\mathbf{u}', p', \theta') + \mathbf{N}(\mathbf{u}', p', \theta') = 0, \quad (5)$$

where \mathbf{L} and \mathbf{N} represent the linear and nonlinear parts of the system (1) with respect to the perturbation fields.

For the LSA, the nonlinear part $\mathbf{N}(\mathbf{u}', p', \theta')$ is neglected and the linearized system $\mathbf{L}(\mathbf{u}', p', \theta') = 0$ is solved by expanding the perturbations into normal modes of the form [14]

$$(\mathbf{u}', p', \theta') = (\hat{\mathbf{u}}(r), \hat{p}(r), \hat{\theta}(r)) \exp[\sigma t + i(\omega t + n\varphi + kz)], \quad (6)$$

where σ , ω , n , and k are, respectively, the temporal growth rate, frequency, azimuthal wave number, and axial wave number of the perturbation flow. The vector $\Psi(r) = (\hat{\mathbf{u}}(r), \hat{p}(r), \hat{\theta}(r))^T$ is the structure function. It satisfies the Sturm-Liouville system:

$$\begin{aligned} \mathcal{L}\Psi(r) &= s\mathcal{B}\Psi(r), \quad \text{with } s = \sigma + i\omega, \\ \Psi\left(\frac{\eta}{1-\eta}\right) &= \Psi\left(\frac{1}{1-\eta}\right) = 0, \end{aligned} \quad (7)$$

where the operators \mathcal{L} and \mathcal{B} are given by

$$\begin{aligned} \mathcal{L} &= \begin{pmatrix} \text{Re}^{-1}(\Delta - r^{-2}) & -2\Omega(1 - \gamma_a \Theta) - 2in\text{Re}^{-1}r^{-2} & 0 & -D & -\gamma_a r \Omega^2 \\ -\Omega D - 2\Omega + 2in\text{Re}^{-1}r^{-2} & \text{Re}^{-1}(\Delta - r^{-2}) & 0 & -inr^{-1} & 0 \\ 0 & 0 & \text{Re}^{-1}(\Delta - r^{-2}) & -ik & 0 \\ D + r^{-1} & in & ik & 0 & 0 \\ D\Theta & 0 & 0 & 0 & \text{Pr}^{-1}\text{Re}^{-1}\Delta \end{pmatrix}, \quad (8) \\ \mathcal{B} &= \begin{pmatrix} 1 & 0 & 0 & 0 & 0 \\ 0 & 1 & 0 & 0 & 0 \\ 0 & 0 & 1 & 0 & 0 \\ 0 & 0 & 0 & 0 & 0 \\ 0 & 0 & 0 & 0 & 1 \end{pmatrix}. \end{aligned} \quad (9)$$

We have introduced the local angular frequency $\Omega = V/r$ and a differential operator $D = d/dr$. The Laplacian operator should be understood as $\Delta = r^{-1}D(rD) - n^2r^{-2} - k^2$.

In the system (7), the coupling of the temperature gradient with the perturbation of the radial velocity ($D\Theta \hat{u}$) is the source of the temperature perturbation which, in turn, couples with the velocity field via the centrifugal buoyancy ($-\gamma_a r \Omega^2 \hat{\theta}$) to amplify the flow perturbation.

Nonlinear analysis can be performed with using the normal mode expansion of the system (5). This method is, however, cumbersome for such a problem [18, 19] so that we use the DNS to obtain nonlinear properties of the flow.

B. Numerical methods

The eigenvalue problem (7) was solved by the Chebyshev spectral collocation method. Each normal mode is expanded into a Chebyshev power series and Eqs. (7) are discretized with the Chebyshev-Gauss-Lobatto collocation points. The resulting generalized eigenvalue problem in matrix form is solved by the generalized Schur decomposition or QZ decomposition to compute eigenvalues and eigenvectors [11].

For the DNS, the governing equations were discretized by a finite-volume method in a cylindrical coordinate system. A second-order central difference method was employed for spatial discretization of the derivatives. A hybrid scheme was used for time advancement: nonlinear terms and cross-diffusion terms were explicitly advanced by a third-order Runge-Kutta scheme, and the diffusion terms were implicitly advanced by the Crank-Nicolson scheme [12, 13]. A fractional step method was employed to decouple the continuity and momentum equations [20]. The fast Fourier transform (FFT) was used to solve the Poisson equation resulting from the fractional step method [20]. The velocity and the temperature were assumed to be periodic in the axial direction (z):

$$\mathbf{u}(r, \varphi, z) = \mathbf{u}(r, \varphi, z + L), \quad \theta(r, \varphi, z) = \theta(r, \varphi, z + L), \quad (10)$$

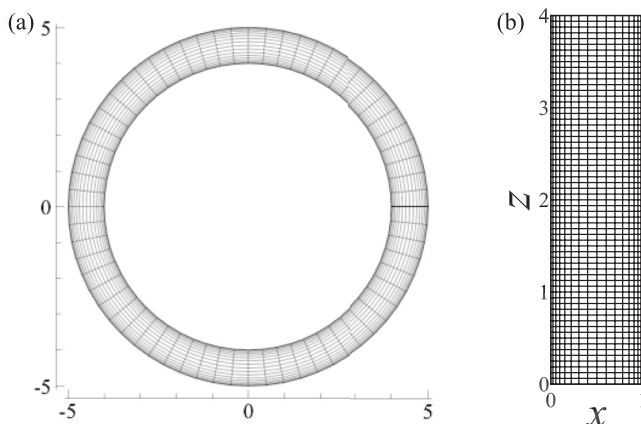


FIG. 2. Grid system (every four grid points is plotted in radial direction for clarity); (a) r - φ plane, (b) r - z plane.

where L is the domain length in the axial direction fixed to $L = 4d$. The number of grid cells used in the present study is $64(r) \times 64(\varphi) \times 64(z)$. The uniform grid was adopted in the azimuthal and axial directions, while grid points clustered close to the cylinder surfaces were used in the radial direction with the minimum grid size $0.005 d$ (Fig. 2).

III. RESULTS

A. Threshold of the instability

The threshold and the nature of instability were determined by both the linear stability analysis and the DNS. Both methods yield the same results within a precision of 0.8% (Table I). For a fixed value of Pr , the critical values of Ta increases with γ_a . At large Pr , the outward heating ($\gamma_a > 0$) induces critical oscillatory modes ($\omega_c \neq 0$), while the critical modes are stationary ($\omega = 0$) in inward heating ($\gamma_a < 0$).

To get a better insight into the effect of the centrifugal buoyancy and the centrifugal force, we have analyzed the spectrum of the eigenvalues of the operator \mathcal{L} , in particular, those corresponding to axisymmetric modes ($n = 0$). Yoshikawa *et al.* [11] showed that, in the inviscid approximation,

TABLE I. Critical parameters and coefficients of the Ginzburg-Landau equation against Pr and γ_a ($\eta = 0.8$).

Pr	γ_a	Ta_c	Ta_c	k_c	ω_c	τ_0	τ_0	ξ_0	c_0	c_g	c_1	l
		(LSA)	(DNA)	(LSA)	(LSA)	(LSA)	(DNS)					
10	-10^{-2}	46.533	46.594	3.134		4.16	4.791	0.269				60.82
	-10^{-3}	47.281	47.231	3.133	0	3.66	3.559	0.270	0	0	0	29.31
	10^{-3}	47.452	47.380	3.132		3.54	3.475	0.270				25.69
	10^{-2}	48.246	48.209	3.132		2.98	3.288	0.270				17.84
50	-10^{-2}	43.996	44.343	3.136	0	17.6	9.59	0.269	0	0	0	1157.24
	10^{-2}	48.292	49.020	3.123	0.008	7.19	3.294	0.271	-0.469	0.002	-0.469	-60.04
100	-10^{-2}	41.337	41.509	3.140	0	51.0	36.326	0.268	0	0	0	2485.11
	-10^{-3}	46.643	47.160	3.133	0	10.5	3.801	0.269	0	0	0	1499.98
	10^{-3}	47.748	47.595	3.128	0.002	7.17	3.527	0.270	-0.951	0.001	-0.951	-53.62
	10^{-2}	47.932	48.905	3.128	0.009	7.21	3.097	0.270	-0.181	0.003	-0.218	-431.22

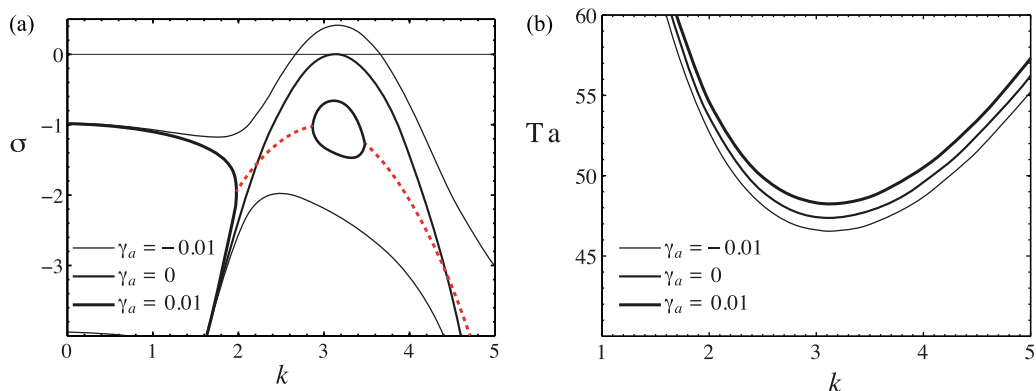


FIG. 3. (a) Variation of the growth rate with the wave number for $Ta = 47.4$ and (b) marginal stability curves for $\eta = 0.8$ and $Pr = 10$ for isothermal case ($\gamma_a = 0$), inward heating ($\gamma_a = -0.01$) and outward heating ($\gamma_a = 0.01$). Stationary and oscillatory modes are shown by solid and broken lines, respectively.

the problem contains two different modes: the centrifugal mode and the temperature mode. For a given value of the radius ratio, the behavior of the critical modes depends on the Prandtl number. Figure 3(a) illustrates the behavior of eigenvalues in the cases of isothermal ($\gamma_a = 0$), inward heating ($\gamma_a = -0.01$), and outward heating ($\gamma_a = 0.01$) at a given set of Pr and Ta ($Pr = 10$, $Ta = 47.4$). The fastest growing modes (i.e., modes with the largest σ) are stationary and axisymmetric and occur at a critical wave number $k_c = 3.13$ in these three cases [Fig. 3(b)]. These modes are centrifugal ones, but their growth rates are modified by the centrifugal buoyancy. As the centrifugal buoyancy enhances and weakens the centrifugal force in inward and outward heating, respectively [14], the growth rate becomes larger and smaller for a negative and positive γ_a compared to the isothermal case. The variation of the growth rate with the criticality parameter $\epsilon = Ta/Ta_c - 1$ and the marginal stability curves for $Pr = 50$ shows that no oscillatory mode is expected near the criticality for inward heating (Fig. 4). In outward heating ($\gamma_a > 0$) where the fluid layer is in stable stratification under the centrifugal gravity field \mathbf{g}_c , oscillatory modes can become critical when γ_a is larger than a certain threshold γ_a^* that depends on η and Pr [14]. The dispersion curves $\sigma = \sigma(k)$ and $\omega = \omega(k)$ computed for $Pr = 50$ at critical conditions ($Ta = Ta_c$) illustrate the merging of the different eigenvalue branches (Fig. 5). Figure 6 shows the variation of the growth rate and the

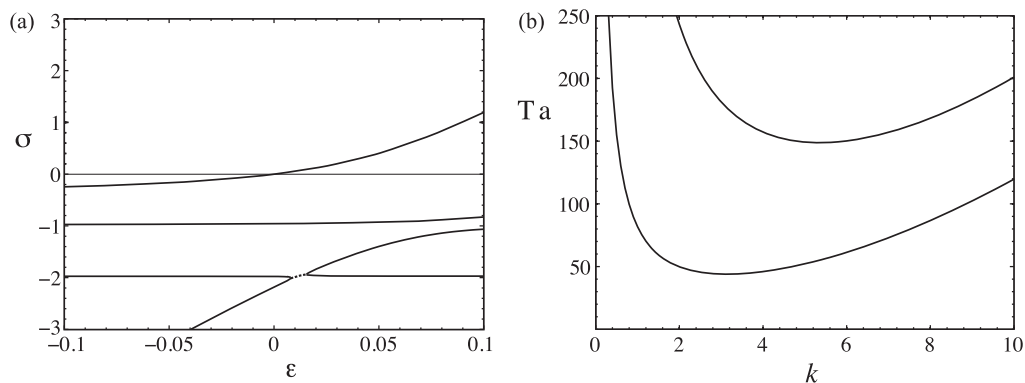


FIG. 4. (a) Variation of the growth rate with the criticality $\epsilon = Ta/Ta_c - 1$ and (b) marginal curves of the first two unstable modes, for $\eta = 0.8$, $Pr = 50$, and $\gamma_a = -0.01$. Branches of stationary and oscillatory modes are shown by solid and broken lines, respectively.

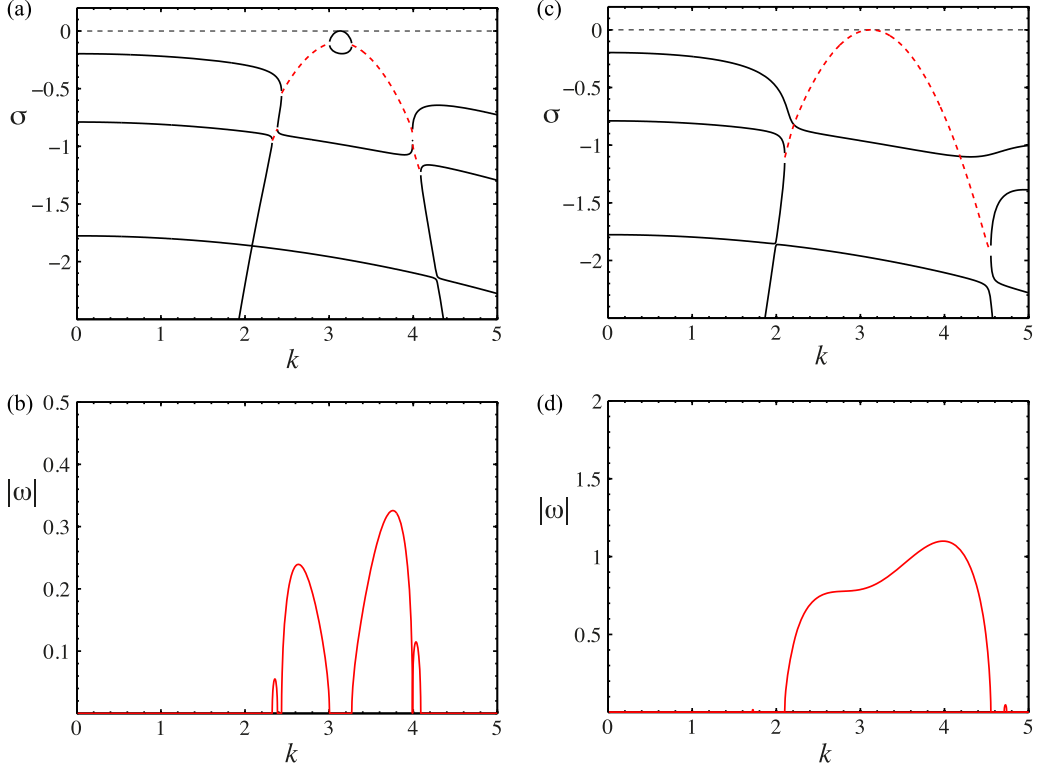


FIG. 5. Variation of the growth rate and the frequency with the wave number k for $\eta = 0.8$ and $\text{Pr} = 50$ at $\text{Ta} = \text{Ta}_c$. The thermal expansion parameter $\gamma_a = 0.001 < \gamma_a^* = 0.002$ in (a) and (b) and $\gamma_a = 0.01 > \gamma_a^*$ in (c) and (d).

frequency with the criticality parameter together with the marginal stability curves and the frequency dispersion curve of oscillatory modes.

In the neighborhood of the instability threshold, the complex linear growth rate $s = \sigma + i\omega$ can be expanded into power series of the axial wave number k :

$$s = \sigma_0 \epsilon + \sigma_1 q^2 + i[\omega_c + \omega_{\text{Ta}} \epsilon + c_g q + \omega_2 q^2] + O(q^3), \quad (11)$$

where $q = (k - k_c)$ and the coefficients are given by the following partial derivatives evaluated at the critical condition:

$$\begin{aligned} \sigma_0 &= \text{Ta}_c \left(\frac{\partial \sigma}{\partial \text{Ta}} \right)_c, & \sigma_1 &= \frac{1}{2} \left(\frac{\partial^2 \sigma}{\partial k^2} \right)_c, & c_g &= \left(\frac{\partial \omega}{\partial k} \right)_c, \\ \omega_{\text{Ta}} &= \text{Ta}_c \left(\frac{\partial \omega}{\partial \text{Ta}} \right)_c, & \omega_2 &= \frac{1}{2} \left(\frac{\partial^2 \omega}{\partial k^2} \right)_c. \end{aligned} \quad (12)$$

B. Complex Ginzburg-Landau equation

The dispersion relation (11) is identical to the linear part of the complex Ginzburg-Landau equation (GLE) describing the amplitude of a Fourier mode e^{ikz} . The GLE, which can describe perturbation flow in its weakly nonlinear regime, is given by [21,22]

$$\tau_0 \left(\frac{\partial A}{\partial t} - c_g \frac{\partial A}{\partial z} \right) = \epsilon(1 + ic_0)A + \xi_0^2(1 + ic_1) \frac{\partial^2 A}{\partial z^2} - l(1 + ic_3)|A|^2 A + g(1 + ic_5)|A|^4 A, \quad (13)$$

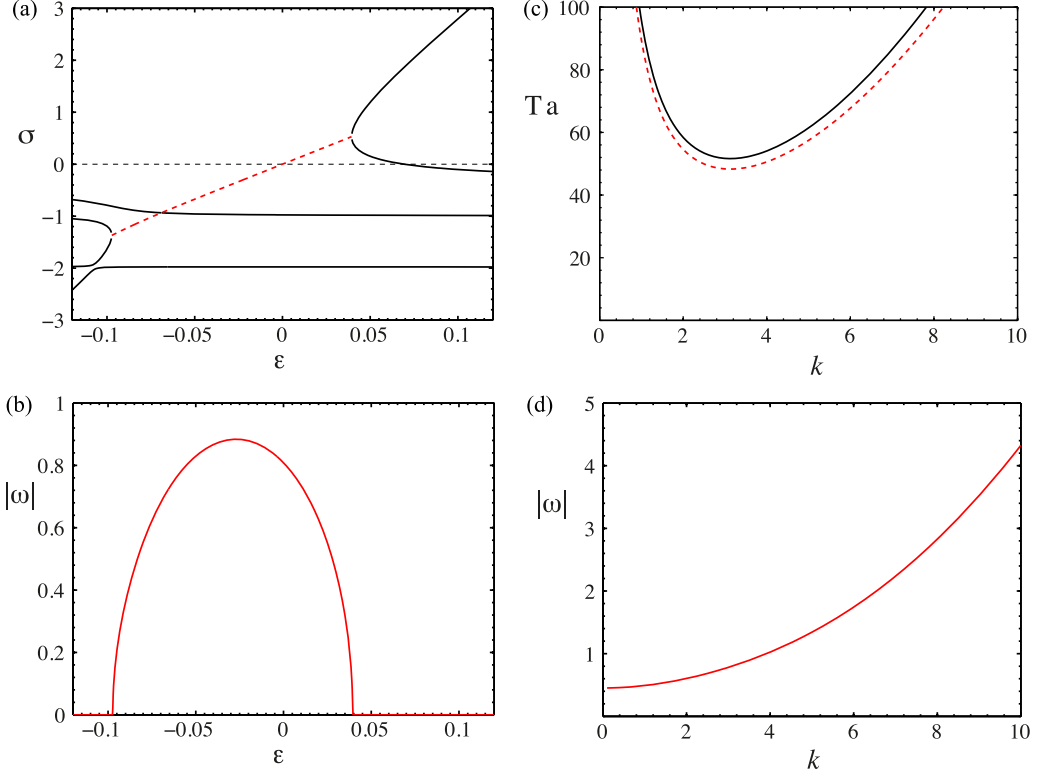


FIG. 6. Stability analysis for $\eta = 0.8$, $\text{Pr} = 50$, and $\gamma_a = 0.01$: Variation of the growth rate (a) and the frequency (b) with the criticality $\epsilon = \text{Ta}/\text{Ta}_c - 1$, marginal curves of the first two unstable modes (c), Variation of the frequency of the oscillatory mode with the wave number, i.e., dispersion relation (d).

where

$$\tau_0 = \frac{1}{\sigma_0}, \quad \xi_0 = \left(-\frac{\sigma_1}{\sigma_0} \right)^{1/2}, \quad c_0 = \frac{\omega_{\text{Ta}}}{\sigma_0}, \quad c_1 = \frac{\omega_2}{\sigma_1}.$$

The parameters τ_0 and ξ_0 represent the characteristic time and the coherence length of perturbation, respectively. For time-dependent perturbations, c_0 and c_1 are the linear dispersion coefficients, and c_g is the group velocity. The third and fourth terms at the right-hand side of Eq. (13) concern the nonlinear state of flow. The constants c_3 and c_5 are nonlinear dispersion coefficients. The Landau constant l determines the nature of the bifurcation from the base flow (3) [23]. If $l > 0$, the bifurcation is supercritical. For stationary perturbation flow, the amplitude saturates at the equilibrium value $A_e = \sqrt{\epsilon/l}$ after a large enough time. If $l < 0$, the bifurcation is subcritical and no saturation is expected for the GLE of the third order. Then, the fifth order nonlinearity, i.e., the fourth term at the right-hand side of Eq. (13), is at least needed for saturation.

The linear coefficients were computed by LSA and the nonlinear coefficient l was extracted from DNS results. For validation of the numerical code, the time constant τ_0 has also been computed by DNS. From the linear growth of the amplitude [Fig. 7(a)], the growth rate σ is determined. The variation of σ in function of the Taylor number Ta gives the constant τ_0 . The results of both LSA and DNS agree quite well with each other (Table I). In the present study, the amplitude of a perturbation mode ($|A|$) was defined as follows:

$$|A| = \frac{1}{2\pi r_m L r_i \Omega_i} \int_0^L \int_0^{2\pi} |u_r(r_m, \varphi, z)| d\varphi dz, \quad \text{where } r_m = \frac{r_i + r_o}{2}. \quad (14)$$

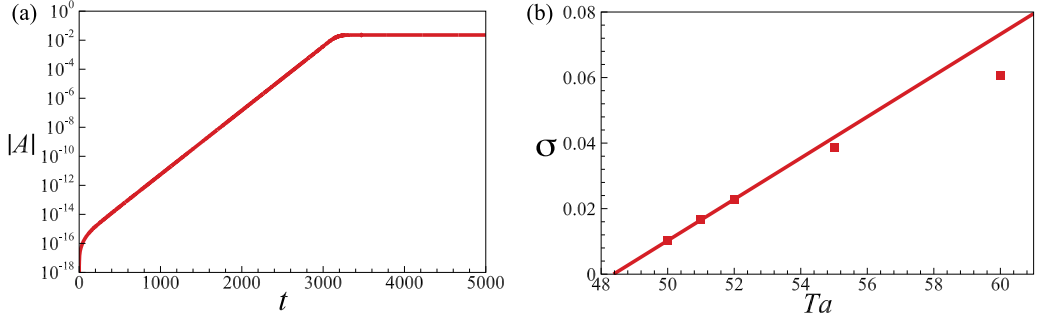


FIG. 7. (a) The growth and saturation of the amplitude of perturbation mode for $Ta = 50$, $Pr = 20$, and $\gamma_a = 0.01$. (b) The growth rate of the instability plotted against Ta for $Pr = 20$, $\gamma_a = 0.01$.

In the DNS, the spatial modulation of the complex amplitude was ignored because of the periodic boundary conditions in the axial direction. The complex amplitude can thus be represented as $A = |A(t)| \exp[i\phi(t)]$ so that the amplitude equation (13) is split into two equations: one for the real amplitude $|A|$ and another for the phase ϕ :

$$\begin{aligned} \tau_0 \frac{d}{dt}(\ln |A|) &= \epsilon - l|A|^2 + g|A|^4 =: f(|A|^2), \\ \tau_0 \frac{d}{dt}(\phi) &= \epsilon c_0 - lc_3|A|^2 + gc_5|A|^4. \end{aligned} \quad (15)$$

The plot of $(d \ln |A|/dt)$ against $|A|^2$ (e.g., Fig. 8) allows us to determine the coefficients l and g [24]: l is given by the slope at the origin $|A|^2 = 0$; g is determined only for subcritical bifurcation from the abscissa $|A_m|^2$ of the maximum of $f(|A|^2)$ [Fig. 8(b)]:

$$l = - \left. \frac{df(|A|^2)}{d|A|^2} \right|_{|A|^2=0}, \quad g = \frac{l}{2|A_m|^2} < 0. \quad (16)$$

The computed values of the coefficients are given in Table I for some values of γ_a and Pr . We found that all the stationary modes appear through a supercritical bifurcation (i.e., with $l > 0$) while oscillatory modes through the subcritical transition. For $Pr = 50$ and 100 , the bifurcation to oscillatory axisymmetric modes is subcritical for $\gamma_a = 0.001$ and 0.01 while the transition to stationary axisymmetric modes is supercritical for all values of Pr . The coherence length ξ_0 is almost independent of Pr for inward and outward heating. The characteristic time τ_0 weakly varies with Pr

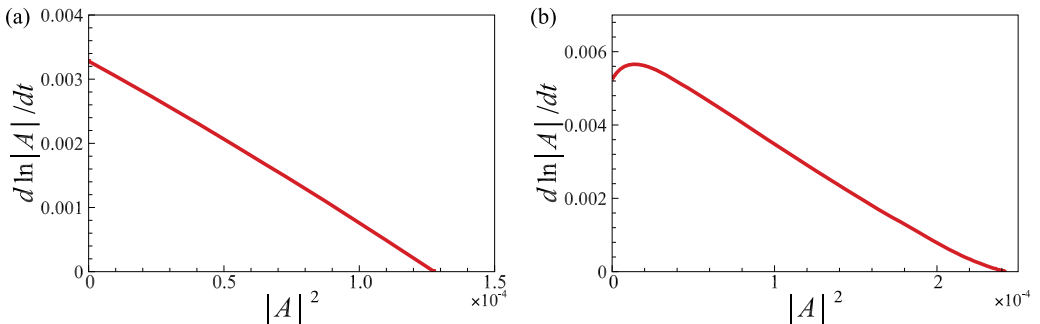


FIG. 8. The derivative of the amplitude logarithm plotted against the square of the amplitude: (a) for $\gamma_a = 0.001$, $Pr = 10$, $Ta = 48$ (supercritical bifurcation); (b) for $\gamma_a = 0.01$, $Pr = 50$, $Ta = 49$ (subcritical bifurcation).

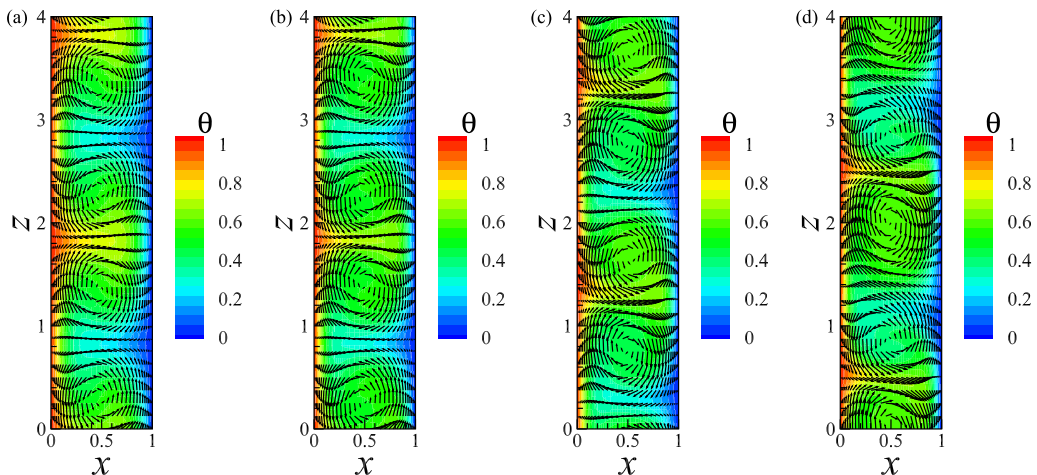


FIG. 9. Instantaneous velocity and temperature fields of flow in the r - z plane for $\text{Pr} = 10$ and $\gamma_a = 0.01$ (the abscissa x is a shifted radial coordinate: $x = r - r_i$): (a) $Ta = 49$, (b) $Ta = 55$, (c) $Ta = 60$, (d) $Ta = 65$.

for $\gamma_a > 0$ while it strongly increases with Pr for $\gamma_a < 0$. Thus, the dependence of the perturbation slowing down near the onset, i.e., the time $\tau = \tau_0/\epsilon$ with Pr , exhibits an asymmetric behavior for inward and outward heating: for a given fluid, the perturbations grow faster in the outward heating than in the inward heating. For the subcritical bifurcation to oscillatory modes for $\gamma_a = 0.01$, we found $g = -2.07 \times 10^6$ for $\text{Pr} = 50$ and $g = -1.79 \times 10^7$ for $\text{Pr} = 100$.

C. Flow patterns

We have performed DNS in both outward and inward heating for $\text{Pr} \in 10, 50, 100$, which were representative for the different modes obtained in LSA. For $\text{Pr} = 10$, axisymmetric stationary counter-rotating vortices are formed in the annulus at the onset of the instability. Figure 9 shows instantaneous velocity fields in the r - z plane together with instantaneous temperature fields for $\gamma_a = 0.01$ and different values of Ta . Figure 10 represents the variation in time and in axial direction of the temperature field for the same parameters as in Fig. 9. As Ta increases, vortices become unstable and for $Ta > 55$, wavy vortex flow sets in with oscillations in time that propagate both in the axial and azimuthal directions (Figs. 9(c), 9(d), 10(c), and 10(d)). This transition scenario of flow patterns is identical for both inward heating ($\gamma_a < 0$) and outward heating ($\gamma_a > 0$) at $\text{Pr} = 10$. It is worthwhile to remind that, for isothermal flow ($\gamma_a = 0$), a wavy vortex flow appears at a similar value of Ta (around $Ta = 57$ for $\eta = 0.8$). Therefore, for small values of Pr , although the radial buoyancy has an influence on the threshold of the first instability, it has no significant effect on the threshold of the secondary instability.

For large values of Pr , a different scenario of flow transitions was found in outward heating ($\gamma_a > 0$). Axial velocity and temperature fields in the midgap cylindrical surface and their space-time diagrams are presented in Figs. 11 and 12, respectively, both for $\text{Pr} = 50$ and $\gamma_a = 0.01$. The instability leads to counter-rotating helical vortices, traveling in the axial direction [Figs. 11(a) and 12(a)]. However, as Ta increases, vortices become stationary and axisymmetric [Figs. 11(b) and 12(b)]. Like in the case of small values of Pr , a further increase of Ta leads to the wavy vortex flow [Figs. 11(c) and 12(c)]. The three-dimensional cores of each vortices can be seen in Fig. 13. On the other hand, for the inward heating ($\gamma_a < 0$), no inclined vortices appeared at the onset Ta_c even at $\text{Pr} = 100$: the instability yields stationary axisymmetric vortices as in the case of low values of Pr (Fig. 14), confirming the stationary nature of the bifurcation predicted by the LSA.

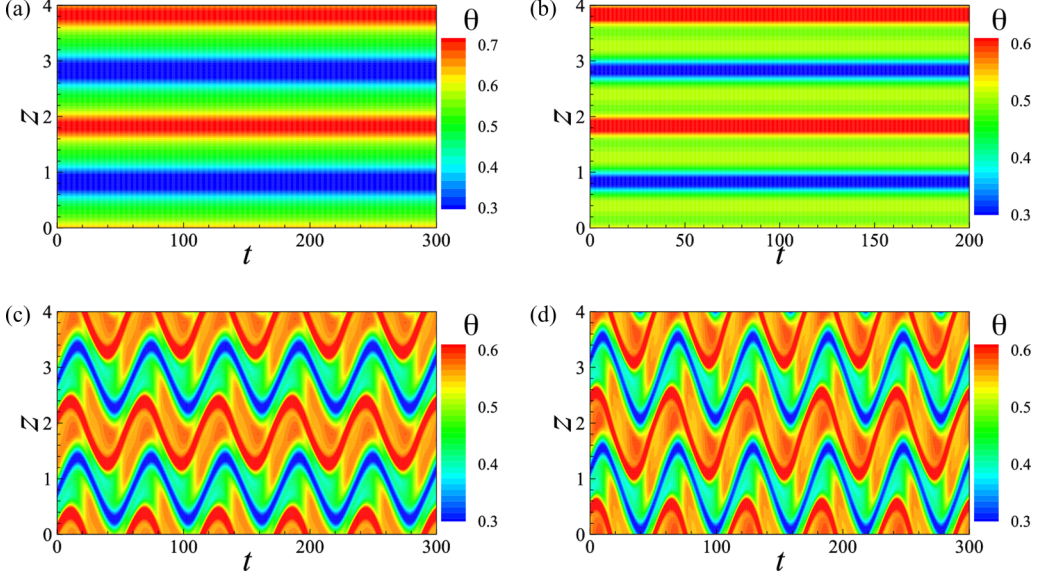


FIG. 10. Space-time diagram of temperature field for $\text{Pr} = 10$ and $\gamma_a = 0.01$ at the midgap $r = r_m$ and a given φ : (a) $\text{Ta} = 49$, (b) $\text{Ta} = 55$, (c) $\text{Ta} = 60$, (d) $\text{Ta} = 65$.

D. Momentum and heat transfer

1. Current density of the angular velocity and pseudo-Nusselt number

Averaging the φ -momentum equation (1c) over time and over a cylindrical surface area $A(r) = 2\pi rL$ yields the current density J^ω of the angular velocity $\omega(t, \mathbf{r}) = u_\varphi/r$. This current density is conserved in the radial direction [25]:

$$\frac{dJ^\omega}{dr} = 0, \quad J^\omega = r^3 \left[\langle u_r \omega \rangle_A - \nu \frac{\partial \langle \omega \rangle_A}{\partial r} \right], \quad (17)$$

where

$$\langle X \rangle_A = \frac{1}{A} \iint_A X r dr d\varphi dz. \quad (18)$$

Figure 15 illustrates the profiles of J^ω for some values of Ta : J^ω is constant across the gap and depends only on the value of Ta for stationary states ($\text{Pr} = 10$, $\gamma_a = -0.01$) as well as for oscillatory states ($\text{Pr} = 100$, $\gamma_a = 0.01$).

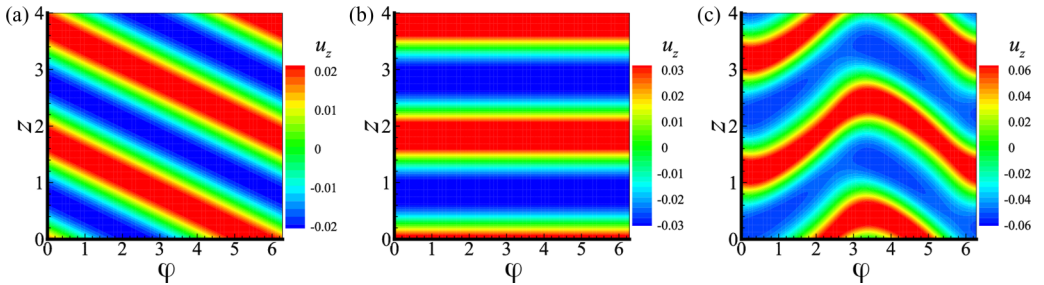


FIG. 11. Instantaneous axial velocity field in the midgap cylindrical surface ($r = r_m$) for $\text{Pr} = 50$, $\gamma_a = 0.01$, and $\eta = 0.8$: (a) $\text{Ta} = 49$, (b) $\text{Ta} = 51$, (c) $\text{Ta} = 60$.

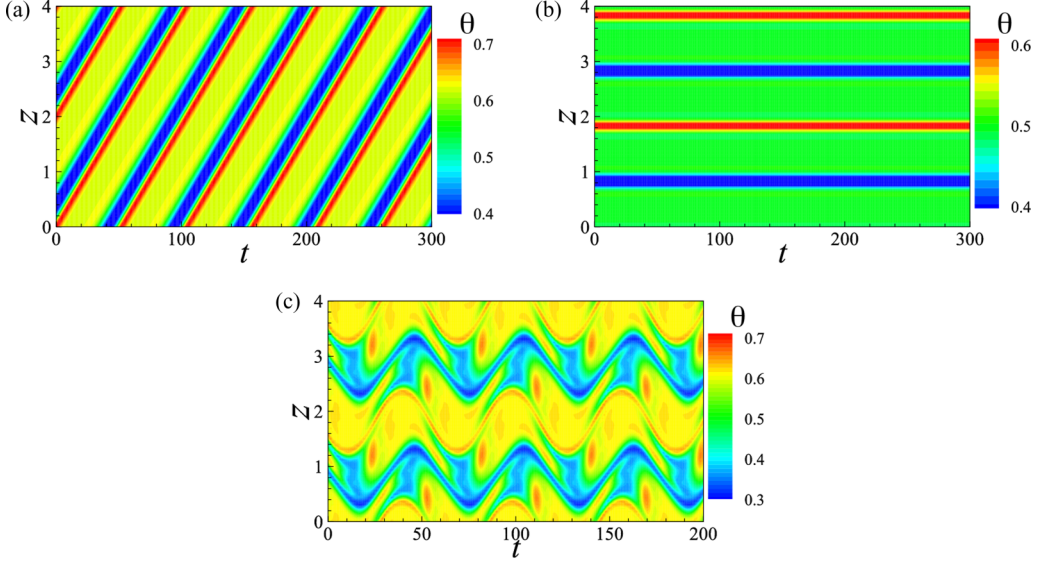


FIG. 12. Space-time diagrams of the temperature for $\text{Pr} = 50$ and $\gamma_a = 0.01$ in the midgap cylindrical surface ($r = r_m$) at a given φ : (a) $Ta = 49$, (b) $Ta = 51$, (c) $Ta = 60$.

The transfer of the transverse momentum in the radial direction can be quantified with the pseudo-Nusselt number defined as follows [25]:

$$N^\omega = \frac{J^\omega}{J_{\text{lam}}^\omega}, \quad (19)$$

where J_{lam}^ω is the current density of angular velocity in the laminar flow (3), which is given by

$$J_{\text{lam}}^\omega = 2\nu B = 2\nu r_i^2 \frac{\Omega_i}{1 - \eta^2}. \quad (20)$$

The pseudo-Nusselt number N^ω is the analog of the Nusselt number Nu of the thermal convection; it measures the efficiency of the transport of the angular velocity in the radial direction by the perturbed flow, compared to the purely molecular transport in the laminar flow [25]. For an isothermal flow, it indicates the dissipation rate (ϵ) through the relation $N^\omega = (1 + \eta)^2 \epsilon / 4$ [13].

The variation of the pseudo-Nusselt number N^ω with Ta is shown in Fig. 16 for $\text{Pr} = 10$ and 100. In the laminar regime, $N^\omega = 1$ and then starts to increase with Ta when the vortices appear in the flow. Only a very weak effect of the radial buoyancy is found, while it affects significantly the flow behavior near the threshold. Indeed, the radial buoyancy has no impact on the N^ω for $Ta \geq 55$, because the centrifugal force effect dominates completely the dynamics of the flow. Moreover, no effect of Pr on the variation of N^ω is detected.

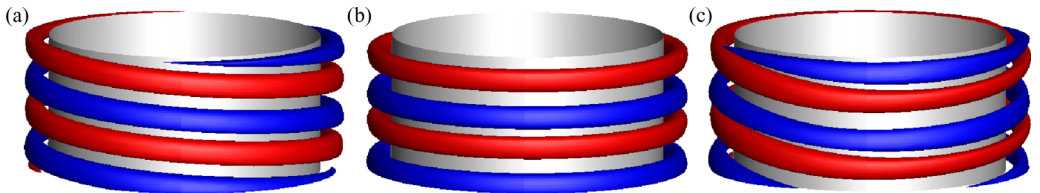


FIG. 13. Cores of the azimuthal vorticity ω_φ for $\text{Pr} = 50$ and $\gamma_a = 0.01$: (a) $Ta = 49$ ($\omega_\varphi = \pm 0.1$), (b) $Ta = 51$ ($\omega_\varphi = \pm 0.16$), (c) $Ta = 60$ ($\omega_\varphi = \pm 0.28$). Blue and red cores are of positive and negative ω_φ .

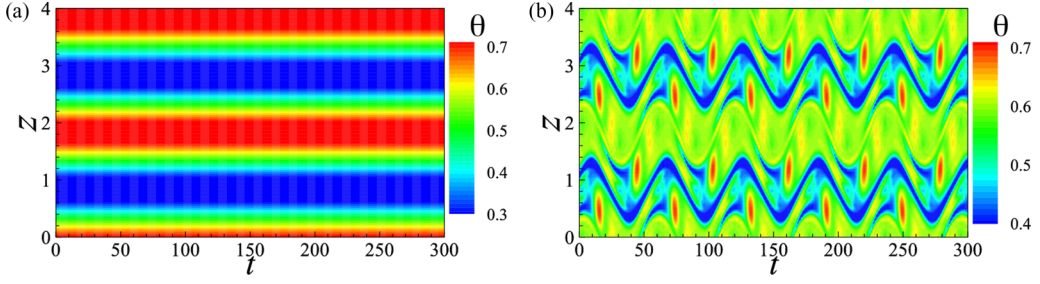


FIG. 14. Space-time diagram of the temperature field for $\text{Pr} = 100$, $\gamma_a = -0.001$ at the midgap $r = r_m$ and a given φ : (a) $\text{Ta} = 47$, (b) $\text{Ta} = 60$.

2. Friction coefficient

The friction coefficient is a dimensionless measure of the torque $\mathbf{M} = M\mathbf{e}_z$ that the fluid exerts on the inner cylinder and it is given by [12,13]

$$C_M = \frac{M}{\rho_0 \pi r_i^2 L (r_i \Omega_i)^2 / 2}. \quad (21)$$

In Fig. 17, the variation of the friction coefficient C_M against Ta is presented for $\text{Pr} = 10$ and 100 together with the coefficient for laminar circular Couette flow given by [12]

$$C_M = \frac{1}{\eta(1+\eta)} \left(\frac{1-\eta}{\eta} \right)^{1/2} \frac{8}{\text{Ta}}. \quad (22)$$

The friction coefficient C_M on the inner cylinder is equal to its laminar flow value (22) for $\text{Ta} \leq 45$, even though the flows are destabilized. This means that weak counter-rotating vortices induced by the centrifugal buoyancy have little effect on the torque. For $\text{Ta} > 45$, C_M depends only weakly on Ta near the critical values: for the inward heating ($\gamma_a < 0$), C_M is larger than that of the outward heating ($\gamma_a > 0$) in the vicinity of Ta_c , because the flow is more unstable, and the magnitude of vortices is stronger for $\gamma_a < 0$. However, for $\text{Ta} \geq 55$, the radial buoyancy does not make any difference in torque. This result is a signature of the weak influence of the radial buoyancy γ_a and the Prandtl number Pr in the radial momentum transfer which is dominated by the centrifugal force.

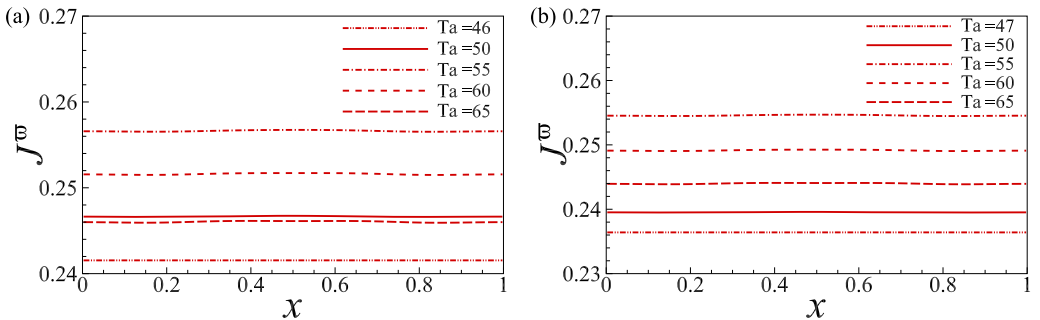


FIG. 15. Variation of the current density of angular velocity J^ω with Ta : (a) $\text{Pr} = 10$, $\gamma_a = -0.01$, (b) $\text{Pr} = 100$, $\gamma_a = 0.01$.

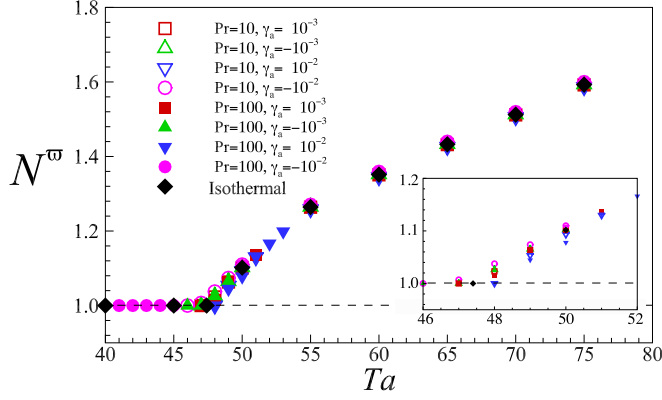


FIG. 16. Variation of angular momentum current with Ta for $Pr = 10$ and 100 . The inset shows the neighborhood of the instability threshold.

3. Radial heat current density and Nusselt number

Averaging the energy equation [Eq. (1e)] on the cylindrical surface (φ, z) yields the conserved radial heat current (J^{th}):

$$\frac{dJ^{th}}{dr} = 0; \quad J^{th} = rj_r^{th}, \quad j_r^{th} = \left\langle u_r \theta - \kappa \frac{\partial \theta}{\partial r} \right\rangle_A. \quad (23)$$

The radial variation of the radial heat current density (J^{th}) is illustrated in Fig. 18 for $Pr = 100$, where J^{th} is shown to be constant across the gap for different values of Ta . The conservation of the radial heat current density suggests that J^{th} is a perfect analog of the current density of the angular velocity J^ω .

The Nusselt number that measures the relative heat transfer of the convective flow across a cylindrical surface of radius r compared to the conductive state is expressed as [12]

$$Nu = \frac{J^{th}}{J_{cond}^{th}}, \quad \text{where} \quad J_{cond}^{th} = \frac{\kappa \Delta T}{\ln \eta}. \quad (24)$$

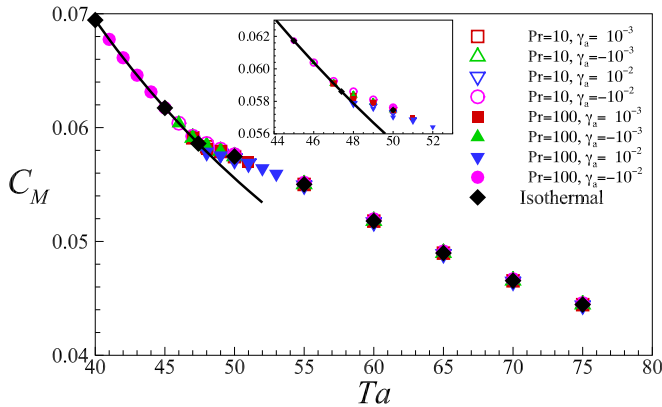


FIG. 17. Total friction coefficient (C_M) against Ta for $Pr = 10$ and 100 . Solid line corresponds to the isothermal laminar flow values of the [Eq. (22)]. The inset shows the neighborhood of the instability threshold.

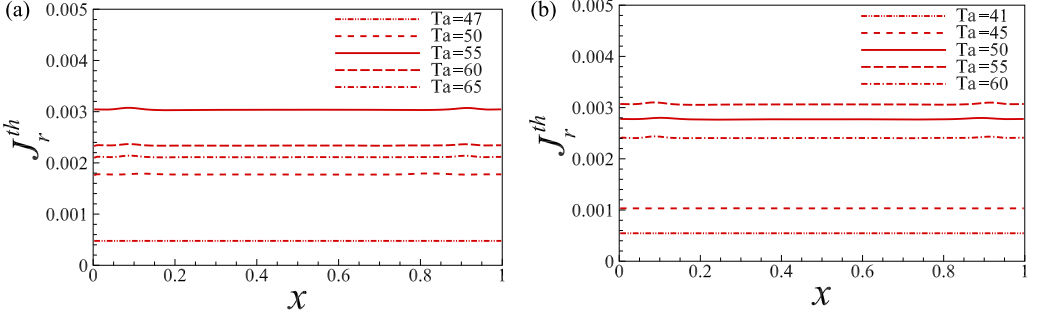


FIG. 18. Radial heat current density across the φ - z plane with Ta for $Pr = 100$; (a) $\gamma_a = 0.01$, (b) $\gamma_a = -0.01$.

The heat transfer at the inner cylinder surface ($u_r = 0$) is given by

$$Nu_i = -\frac{\eta \ln \eta}{1 - \eta} \left(\frac{\partial \theta}{\partial r} \right)_{r=r_i}. \quad (25)$$

In order to illustrate the effect of the centrifugal buoyancy on heat transfer, we present the variation of Nu_i with Ta for $Pr = 10$ and 100 for the inward heating and the outward heating in Fig. 19. For $Pr = 10$, the critical modes are stationary axisymmetric independently on the sign of γ_a , while for $Pr = 100$, the critical modes are stationary axisymmetric for inward heating and oscillatory axisymmetric for outward heating (Figs. 14, 20, and 21). In contrast to the coefficient of the angular velocity transfer N^ω , which depends neither on Pr nor on γ_a , the heat transfer coefficient Nu_i is very sensitive to Pr : for a given value of Ta ($> Ta_c$), Nu_i is larger for $Pr = 100$ than for $Pr = 10$. For $Pr = 10$, the heat transfer is characterized by a monotonic increase with Ta from $Nu_i = 1$ at the onset Ta_c . The influence of the centrifugal buoyancy (γ_a) is limited to the neighborhood of the instability threshold [Fig. 19(a)] and disappears for large values of Ta . The asymmetry induced by the centrifugal buoyancy on the threshold does not appear in the heat transfer, i.e., $Nu_i(-\gamma_a) \approx Nu_i(\gamma_a)$ except in the close neighborhood of the instability threshold where the slope of the curve $Nu_i = Nu_i(Ta)$ exhibits a small difference. The heat transfer is mainly ensured by the vortices generated by the centrifugal force. Moreover, the appearance of the wavy vortex modes limits the growth of the heat transfer.

For $Pr = 100$, the curves of heat transfer $Nu_i(Ta)$ have different slopes near the instability thresholds [$Ta_c(-\gamma_a) \neq Ta_c(\gamma_a)$] but quickly coincide around $Ta = 48$ for $\gamma_a = \pm 10^{-3}$ and $Ta = 52$ for $\gamma_a = \pm 10^{-2}$ [Figs. 19(b) and 19(c)]. The coincidence of these curves corresponds to the disappearance of the oscillatory mode in the benefit of the stationary modes for $\gamma_a > 0$ as stated before. The slope of $Nu_i(Ta)$ curve depends on the sign and the intensity of heating, i.e., on γ_a . The asymmetry of the heat transfer is clear in this case because of different nature of vortices that are formed at the threshold (Figs. 20 and 21). The Nusselt number due to nonaxisymmetric vortices for $\gamma_a > 0$ is lower than that due to axisymmetric vortices for $\gamma_a < 0$ near the Ta_c . This difference is due to the axial flow which drifts vortices in the axial direction and diminishes the heat transfer in the radial direction. The growth of the heat transfer is limited by the appearance of the wavy vortex mode which is associated with a decrease of $\Delta Nu_i \simeq -1$. To explain this decrease of Nu_i , we have analyzed separately the convective and diffusive contributions to J^{th} . We found that the convective contribution increases with Ta for all values of Pr while the diffusive contribution may change when the wavy vortex sets in (Fig. 22) depending on Pr : for $Pr = 10$, the slope $(\partial \theta / \partial r)$ of the mean temperature profile is weakly affected by the wavy mode while for $Pr = 100$, it increases, reducing the diffusive contribution to the radial current density and therefore Nu_i . One may mention that there is no decrease in the curve $N^\omega(Ta)$ when the transition to wavy mode occurs, since N^ω is independent on Pr .

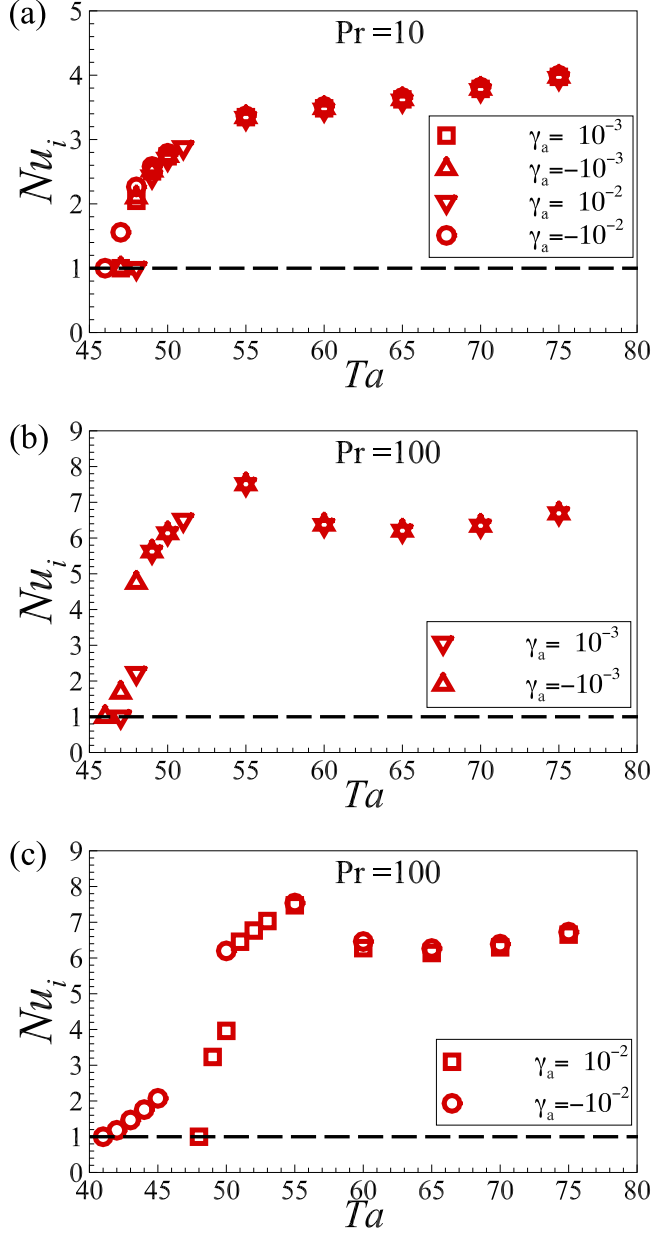


FIG. 19. Variations of heat transfer coefficients at the inner cylinder with Ta for different values of Pr and γ_a . (a) $Pr = 10$, $\gamma_a = \{\pm 10^{-3}, \pm 10^{-2}\}$, (b) $Pr = 100$, $\gamma_a = \pm 10^{-3}$, and (c) $Pr = 100$, $\gamma_a = \pm 10^{-2}$

E. Variation of kinetic energy

From the momentum equations [Eqs. (1b)–(1d)], the variation rate of the kinetic energy per unit volume $E_k = \langle \mathbf{u}^2/2 \rangle_V$ can be derived by averaging over the whole fluid volume. It is expressed as [12]

$$\frac{dE_k}{dt} = -\langle \alpha \theta r u_r \varpi^2 \rangle_V + \frac{2\Omega_i}{r_o^2 - r_i^2} J^\varpi - \epsilon, \quad \text{where} \quad \langle X \rangle_V = \iiint_C X r dr d\varphi dz. \quad (26)$$

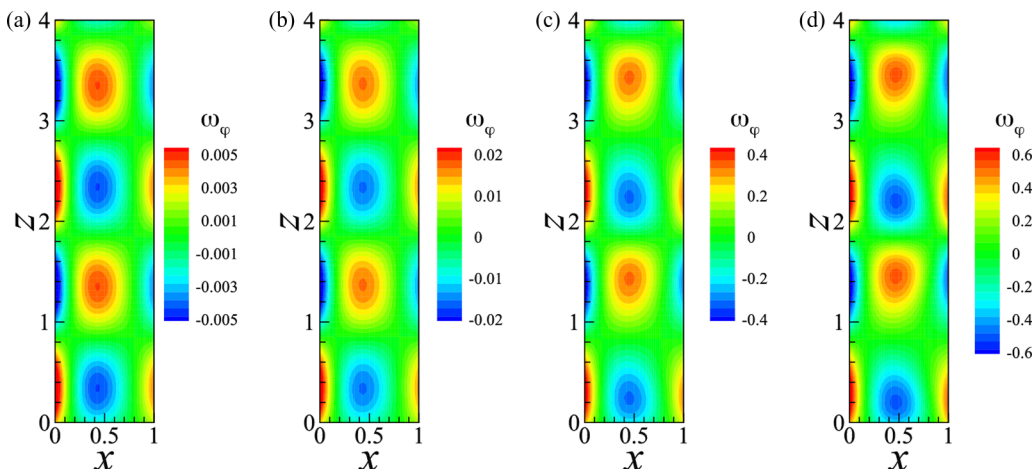


FIG. 20. Contours of azimuthal vorticity (ω_φ) in the annulus for $\text{Pr} = 100$ and $\gamma_a = -0.01$ with different values of Ta ; (a) $Ta = 42$, (b) $Ta = 45$, (c) $Ta = 50$, (d) $Ta = 55$.

The first, second, and third terms on the right-hand side of (26) are the contributions of the centrifugal buoyancy, the radial transport of angular velocity, i.e., the power from torque, and viscous energy dissipation, respectively. We computed these terms for different values of Ta in the outward (Table II) and inward heating (Table III). The dissipation rate (ϵ) is mainly balanced by the radial transport of angular velocity (J^ω). The order of magnitude of the centrifugal buoyancy term remains very small compared to that of the other terms.

In Fig. 23, we plotted the radial profiles of the right-hand side terms of Eq. (26) to identify the balance between each terms. While the contribution from the radial transport of the angular momentum is a constant for r , as previously shown, the dissipation rate has a maximum value on the inner cylinder and a minimum value in the middle of gap. It reveals that the kinetic energy is lost near the inner cylinder surface, and it is gained in the middle of gap.

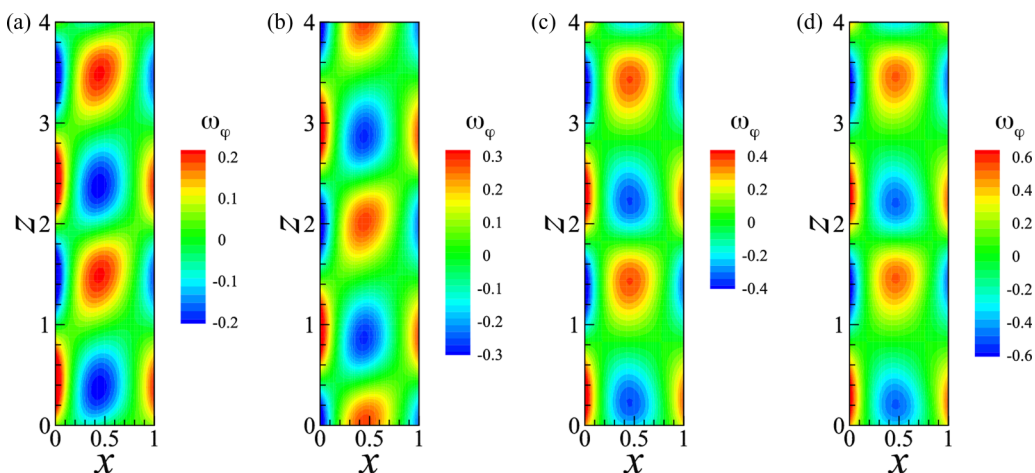


FIG. 21. Contours of azimuthal vorticity (ω_φ) in the annulus for $\text{Pr} = 100$ and $\gamma_a = 10^{-2}$ with different values of Ta ; (a) $Ta = 49$, (b) $Ta = 50$, (c) $Ta = 51$, (d) $Ta = 55$. (for $Ta \in \{49, 50\}$ the modes are non-axisymmetric vortices, for $Ta \in \{51, 55\}$ they are axisymmetric vortices).

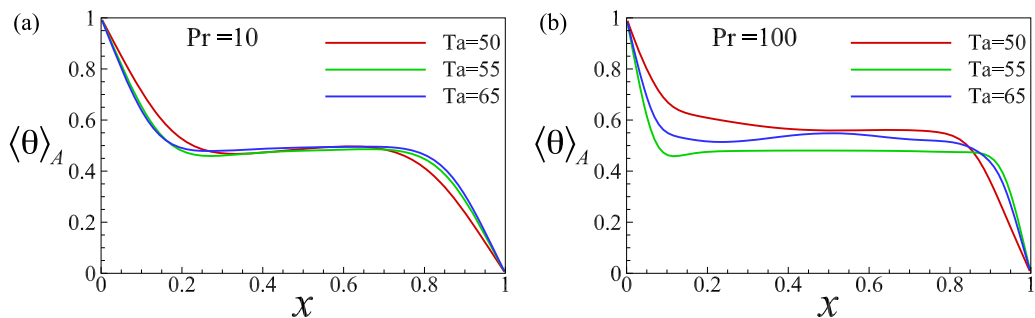


FIG. 22. Radial profiles of the mean temperature for $\gamma_a = 0.01$: (a) $\text{Pr} = 10$, (b) $\text{Pr} = 100$. The abscissa x is a shifted radial coordinate: $x = r - r_i$.

IV. DISCUSSION

The effect of the radial temperature gradient on heat transfer between the two coaxial cylinders of a differentially rotating annulus has been computed both in the LSA and DNS for sets of parameters: $\gamma_a = \pm 0.001, \pm 0.01$ and $\text{Pr} = 10, 50, 100$. The gravitational acceleration was neglected (\mathbf{g}). There is a good agreement between the critical values from both methods. The results of the LSA for different values of γ_a and Pr can be found in Ref. [14]. The centrifugal buoyancy is responsible for the thermal convection while the centrifugal force is responsible for Taylor-Couette instability. The inward heating destabilizes the flow because the centrifugal buoyancy reinforces the action of centrifugal force while the outward heating stabilizes the flow because the centrifugal buoyancy is opposite to the centrifugal force. In the latter situation, above the value of Pr^* , inertial waves are excited and their frequency scales with the Brunt-Väisälä frequency if the viscous damping is ignored [14]. The present study aimed to complete the former LSA results and to investigate the stability of the critical modes and the associate flow structures. In particular, we have analyzed the effect of the parameter γ_a on momentum and heat transfer. In inward heating, the critical mode is the centrifugal mode which remains axisymmetric and stationary (the Taylor vortex mode). A focus has been made on the growth rate of the first two modes in order to identify those associated to oscillatory and stationary temporal behavior in the case of outward heating. The curves of the growth rate and the marginal stability curves have been analyzed, especially in the neighborhood of the threshold. The coefficients of the nonlinear complex Ginzburg-Landau equation have been computed. The stationary axisymmetric modes occur via a supercritical bifurcation while oscillatory axisymmetric modes occur via a subcritical bifurcation.

TABLE II. Contribution terms to the variation rate of the kinetic energy for $\text{Pr} = 10$ and $\gamma_a = 0.01$, $\eta = 0.8$.

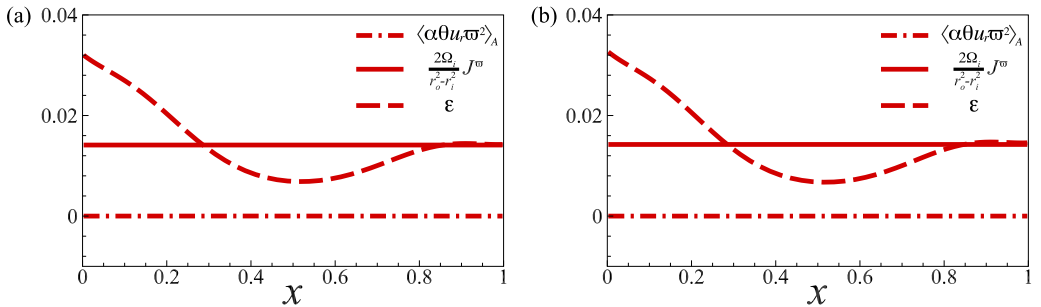
Ta	$-\langle \alpha \theta r u_r \varpi^2 \rangle_V$ ($\times 10^{-6}$)	$\frac{2\Omega_i}{r_o^2 - r_i^2} J^\sigma$ ($\times 10^{-2}$)	ϵ ($\times 10^{-2}$)	E_k ($\times 10^{-2}$)
48	0.0	1.2860	1.2860	8.28897
49	-1.5836	1.3269	1.3264	8.24823
50	-2.2219	1.3495	1.3487	8.21062
55	-4.1847	1.4128	1.4109	8.00485
60	-4.8164	1.3833	1.3803	7.89552
65	-5.2459	1.3544	1.3503	7.78169
70	-5.5752	1.3280	1.3232	7.66805
75	-5.8436	1.3058	1.3004	7.55183

TABLE III. Contribution terms to the variation rate of the kinetic energy for $\text{Pr} = 100$ and $\gamma_a = -0.01$, $\eta = 0.8$.

Ta	$-\langle \alpha \theta r u_r \varpi^2 \rangle_V$ ($\times 10^{-8}$)	$\frac{2\Omega_i}{r_o^2 - r_i^2} J^\varpi$ ($\times 10^{-2}$)	ϵ ($\times 10^{-2}$)	E_k ($\times 10^{-2}$)
41	0.0	1.5056	1.5056	8.28897
42	1.3458	1.4698	1.4698	8.28896
45	7.6977	1.3721	1.3721	8.28882
50	1.6469	1.3672	1.3667	8.19616
55	3.2642	1.4243	1.4230	7.99086
60	4.0720	1.3970	1.3948	7.87574
65	4.5065	1.3657	1.3626	7.76390
70	4.9056	1.3379	1.3341	7.65146
75	5.1916	1.3148	1.3104	7.53564

When Ta was increased, the stationary axisymmetric modes bifurcate to wavy vortex mode, while the oscillatory modes first become stationary and then bifurcate to wavy vortex mode. The transition from oscillatory modes to stationary modes, i.e., the disappearance of the time dependence, suggests that the oscillatory modes are associated with a convective instability. In fact, the oscillatory modes are the manifestation of inertial waves due to the positive radial stratification of density in the centrifugal gravity field. The stationary axisymmetric modes are the result of an absolute instability. The complex Ginzburg-Landau equation yields a framework for the transition from the convective to absolute instability in a finite box [26]. Using this model, we found that for $\gamma_a = 10^{-2}$, the frequency vanishes at a small value of ϵ : $\epsilon = 0.011$ for $\text{Pr} = 50$ and $\epsilon = 0.005$ for $\text{Pr} = 100$.

While the intensity of the centrifugal buoyancy has a significant effect on the threshold and the nature of the critical modes, DNS show that its effect on higher states and on momentum transfer is very weak. We have found that the radial current density of the angular velocity and the radial heat current are independent of the radius, in agreement with the theory developed in Ref. [25] for periodic boundary conditions. However, this should not be the case for nonperiodic boundary conditions. Moreover, the effect of the centrifugal buoyancy on the heat transfer depends on the value of Pr: for $\text{Pr} < \text{Pr}^*$ (with Pr^* being the value above which the oscillatory modes become critical [14]), the modes are mainly driven by the centrifugal force and the heat transfer is not affected by the centrifugal buoyancy [Fig. 19(a)]. For $\text{Pr} > \text{Pr}^*$, the centrifugal buoyancy sensibly modifies the heat transfer in the neighborhood of the threshold. For large values of Ta, its effects become reduced [Fig. 19(b)]. The coefficient of the radial transfer of the angular momentum does not depend on the Pr, and not on γ_a away from the threshold. This means that the radial transfer of the angular momentum remains dominated by the centrifugal force. On the other hand, the coefficient of the heat


 FIG. 23. Radial profiles of different terms of the kinetic energy balance equation (26) for Ta = 55: (a) Pr = 10, $\gamma_a = 0.01$, (b) Pr = 100, $\gamma_a = -0.01$. The abscissa x is a shifted radial coordinate: $x = r - r_i$.

transfer at the inner cylinder Nu_i depends on the diffusive properties of the fluid through Pr and on the flow regime. While it increases from the value of the laminar state $Nu_i = 1$ to about $Nu_i \sim 7$, it decreases when the vortex flow appears and reduces the slope of the mean temperature radial profile at the inner cylinder surface. The heat transfer Nu_i remains very important compared to the radial momentum N^ϖ .

The power from the centrifugal buoyancy is much smaller than that from the centrifugal force. It is negative for outward heating, stabilizing the flow to delay the instability. It takes positive values for inward heating, having destabilizing effects. While the power of the centrifugal force is constant in the gap, the viscous dissipation rate of the kinetic energy is more important near the rotating inner cylinder and very weak in the central part of the gap. The centrifugal force power and the dissipation rate are equal to each other at the surface of the outer fixed cylinder. The DNSs have confirmed the disymmetry between inward and outward heating in the differentially rotating annulus. It has shown that the effect of the centrifugal buoyancy is limited to the neighborhood of the threshold. When a large temperature difference is applied to the fluid, the Boussinesq approximation should be relaxed. The above mentioned weak effects of the centrifugal buoyancy may be altered by this relaxation. This remains an open question.

V. CONCLUSION

In the present study, the circular Couette flow in a cylindrical annulus with rotating inner cylinder and fixed outer cylinder has been studied numerically for representative values of the Prandtl number to clarify the effect of the radial buoyancy induced by a radial temperature gradient on flow bifurcation and on heat transfer. The gravitation acceleration was neglected. The linear stability analysis has been revisited by investigation of the eigenvalue spectrum which shows the coexistence of the different modes in the outward heating: the temperature mode and the centrifugal mode. The interaction between these modes is responsible for the oscillatory modes in outward heating. The reduction of the onset for inward heating is the result of the reinforcement of the centrifugal force by the centrifugal buoyancy. For all situations, the transition to stationary vortices is found to be supercritical while that to oscillatory modes is subcritical. The oscillatory modes disappear when Ta is increased further away from the threshold. The centrifugal force dominates the centrifugal buoyancy and the flow retrieves the classic transition scenario of the isothermal Couette flow from Taylor to wavy vortices. The effect of the centrifugal buoyancy on the torque is found only in the vicinity of the critical Taylor number Ta_c : the friction coefficient (C_M) and the pseudo-Nusselt number (N^ϖ) are dependent on Ta_c . Inward heating causes an enhancement on heat transfer near Ta_c , resulting from the onset of counter-rotating vortices. Outward heating reduces the heat transfer as a consequence of its stabilizing effect on the flow. The behavior of the Nu_i with Ta highlights the disymmetry between the inward and outward heating. For large values of Pr , the heat transfer coefficient diminishes as soon as the wavy vortex mode sets in because of the change of the thermal boundary layer. The dissipation of the kinetic energy is more important in the vicinity of the inner cylinder. It is weaker in the middle of the gap where the centrifugal power is dominant. The contribution of the power from the centrifugal buoyancy is negligibly small in the evolution of the perturbation flow kinetic energy.

ACKNOWLEDGMENTS

The present work has benefited from a partial support from the French Spatial Agency (CNES) and from the French National Research Agency (ANR) through the program "Investissements d'Avenir (No. ANR-10LABX-09-01)," LABEX EMC³. C.K. has benefited from a financial support from the French National Research Agency (ANR) through the program "TRANSFLOW"(ANR-13-BS09-0025-02). A.M. was supported by a doctoral fellowship from the Region Normandie. H.N.Y. acknowledges financial support from the French National Center for Scientific Research (CNRS) through the program PEPS-PTI OndInterGE.

- [1] K. M. Becker and J. Kaye, The influence of a radial temperature gradient on the instability of fluid flow in an annulus with an inner rotating cylinder, *Trans. ASME: J. Heat Transfer* **84**, 106 (1962).
- [2] H. A. Snyder and S. K. F. Karlsson, Experiments on the stability of Couette motion with a radial thermal gradient, *Phys. Fluids* **7**, 1696 (1964).
- [3] H. S. Takhar, T. J. Smith, and V. M. Soundalgekar, Effects of radial temperature gradient on the stability of flow of a viscous incompressible fluid between two rotating cylinders, *J. Math. Anal. Appl.* **111**, 349 (1985).
- [4] K. S. Ball and B. Farouk, A flow visualization study of the effects of buoyancy on Taylor vortices, *Phys. Fluids A* **1**, 1502 (1989).
- [5] K. S. Ball, B. Farouk, and V. C. Dixit, An experimental study of heat transfer in a vertical annulus with a rotating inner cylinder, *Int. J. Heat Mass Transfer* **32**, 1517 (1989).
- [6] H. S. Takhar, V. M. Soundalgekar, and M. A. Ali, Effects of radial temperature gradient on the stability of a narrow-gap annulus flow, *J. Math. Anal. Appl.* **152**, 156 (1990).
- [7] M. Ali and P. D. Weidman, On the stability of circular Couette flow with radial heating, *J. Fluid Mech.* **220**, 53 (1990).
- [8] V. M. Soundalgekar, H. S. Takhar, and M. A. Ali, Effects of a radial temperature gradient on the stability of a wide-gap annulus, *Int. J. Energ. Res.* **14**, 597 (1990).
- [9] C.-H. Kong and I.-C. Liu, The stability of nonaxisymmetric circular Couette flow with a radial temperature gradient, *Phys. Fluids* **6**, 2617 (1994).
- [10] M. Jenny and B. Nsom, Primary instability of a Taylor-Couette flow with a radial stratification and radial buoyancy, *Phys. Fluids* **19**, 108104 (2007).
- [11] H. N. Yoshikawa, M. Nagata, and I. Mutabazi, Instability of the vertical annular flow with a radial heating and rotating inner cylinder, *Phys. Fluids* **25**, 114104 (2013).
- [12] C. Kang, K.-S. Yang, and I. Mutabazi, Thermal effect on large-aspect-ratio Couette–Taylor system: numerical simulations, *J. Fluid Mech.* **771**, 57 (2015).
- [13] R. Guillermin, C. Kang, C. Savaro, V. Lepiller, A. Prigent, K.-S. Yang, and I. Mutabazi, Flow regimes in a vertical Taylor–Couette system with a radial thermal gradient, *Phys. Fluids* **27**, 094101 (2015).
- [14] A. Meyer, H. N. Yoshikawa, and I. Mutabazi, Effect of the radial buoyancy on a circular Couette flow, *Phys. Fluids* **27**, 114104 (2015).
- [15] F. H. Busse, Convection driven zonal flows and vortices in the major planets, *Chaos* **4**, 123 (1994).
- [16] J. M. Lopez, F. Marques, and M. Avila, The Boussinesq approximation in rapidly rotating flows, *J. Fluid Mech.* **737**, 56 (2013).
- [17] O. N. Kirillov and I. Mutabazi, Short-wavelength local instabilities of a circular Couette flow with radial temperature gradient, *J. Fluid Mech.* **818**, 319 (2017).
- [18] P. Laure and I. Mutabazi, Nonlinear analysis of instability modes in the Taylor-Dean system, *Phys. Fluids* **6**, 3630 (1994).
- [19] A. Recktenwald, M. Lücke, and H. W. Müller, Taylor vortex formation in axial through-flow: Linear and weakly nonlinear analysis, *Phys. Rev. E* **48**, 4444 (1993).
- [20] J. Kim and P. Moin, Application of a fractional-step method to incompressible Navier-Stokes equations, *J. Comput. Phys.* **59**, 308 (1985).
- [21] P. Manneville, *Dissipative Structures and Weak Turbulence* (Academic Press, New York, 1990).
- [22] M. C. Cross and P. C. Hohenberg, Pattern formation outside of equilibrium, *Rev. Mod. Phys.* **65**, 851 (1993).
- [23] L. D. Landau and E. M. Lifshitz, *Mechanics*, 3rd ed., Landau and Lifshitz Course of Theoretical Physics Vol. 1 (Elsevier Butterworth-Heinemann, Burlington, MA, 1984).
- [24] G. J. Sheard, M. C. Thompson, and K. Hourigan, From spheres to circular cylinders: the stability and flow structures of bluff ring wakes, *J. Fluid Mech.* **492**, 147 (2003).
- [25] B. Eckhardt, S. Grossmann, and D. Lohse, Torque scaling in turbulent Taylor-Couette flow between independently rotating cylinders, *J. Fluid Mech.* **581**, 221 (2007).
- [26] S. M. Tobias, M. R. E. Proctor, and E. Knobloch, Convective and absolute instabilities of fluid flows in finite geometry, *Physica D (Amsterdam)* **113**, 43 (1998).